Lucie Moreau
Patricia Sánchez Romero

BME Paris
BioMedical Imaging Track

Medical Image Analysis – Mini-Project

Pore segmentation of the lamina cribrosa for glaucoma assessment

Contents

Code availability

All code for this project has been uploaded to GitHub and is available for anyone to view and explore. Click here to acess the folder.

Introduction

Glaucoma, a leading cause of irreversible blindness worldwide, encompasses a range of disorders characterized by optic nerve damage. Among these, Primary Open-Angle Glaucoma (POAG) is a significant subset, marked by progressive visual field loss. It is distinguished by an open anterior chamber angle and elevated intraocular pressure (IOP) without any underlying disease. When an identifiable cause for the elevated IOP is present, the condition is classified as secondary glaucoma.

The lamina cribrosa (LC) plays a critical role in the optic nerve head, providing nutrition to the retinal nerve fiber bundles (RNFBs) through its connective tissue structure. Elevated IOP can cause deformation of the lamina cribrosa pores, disrupting the axonal arrangement, oxygenation, and blood flow necessary for maintaining optic nerve function. Understanding these changes is pivotal for advancing the diagnosis and treatment of POAG. However, the state of the art in this area remains limited, with few articles and recent observations shedding light on these processes.

To address this challenge, we utilized a Flood Illumination Adaptive Optics (FIAO) camera for imaging the optic nerve head. This imaging technique offers high-resolution images with a flashed flood source at 850 nm, capturing a 4° × 4° retinal area (equivalent to 1.2 mm × 1.2 mm) with a lateral resolution of 2 µm. Imaging is conducted in a dark room to facilitate high-quality capture without the need for pharmacological pupil dilation. Nonetheless, pores of the LC might be obscured by microstructures, which decrease the visibility of the region of interest (ROI), i.e., the pores, and thus their segmentation. Figure 1 shows an example of this phenomenon and illustrates the challenge of deciding which structures were relevant.

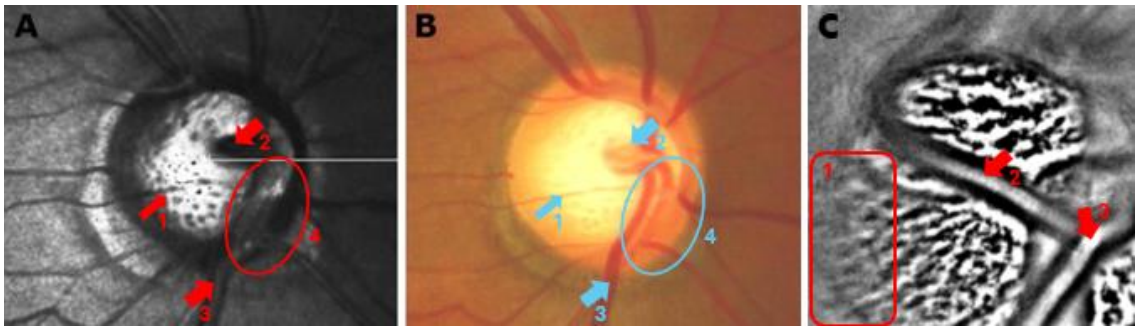

Figure 1: Comparison between grayscale (A) and color (B) confocal scanning laser ophthalmoscopic images with a sample from our dataset's FIAO images (C). Some regions are highlighted with arrows or shapes to indicate the presence of microstructures of the optic nerve head and the regions they obscure, which are not considered as part of the region of interest. In A and B, 1 is a thin blood vessel that may hinder pore detection, 2 is the region where vessels connect, which appears as a shadow in the grayscale image, 3 is a large blood vessel that continues around region 4, which has other blood vessels that appear as shadows in the grayscale image instead. In B, we can see the pores of the LC, many of which are blurred. Such blurring resembles that of region 1 in C. Similarly, structures resembling blood vessels and forming shadows are highlighted by arrows 2 and 3.

The goal of this project was not to determine whether an image came from a glaucoma patient, but simply to segment the pores of interest for each lamina as well as possible.

Methods

Loading Dataset

For our study, we employed a database consisting of ten grayscale images and their associated ground truth annotations. The database exhibits variations in contrast, morphology, the presence of black rectangles, noise, and image centering. The ground truth, provided as binary MATLAB files, was hand-drawn by ophthalmologists.

From the set of ten images, we selected two (LC001 and LC003) that are initially quite distinct. These were chosen to illustrate the results at each step of our method and to capture the broadest possible range of image variations.

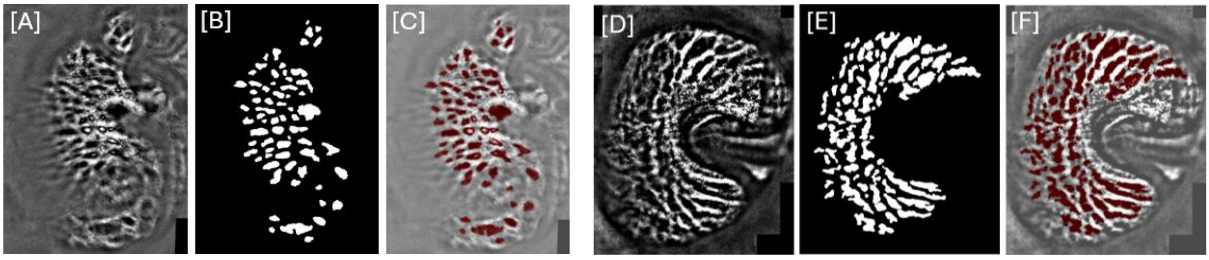

Figure 2: [A] Original image LC001, with its [B] Ground truth, and the [C] Ground truth (in red) displayed on the original grayscale image. [D] Original image LC003, with its [E] Ground truth, and the [F] Ground truth (in red) displayed on the original grayscale image.

Dataset Splitting

To determine the optimal parameters for each method and evaluate their accuracy, we divided our set of ten images into a training set and a test set. An ideal split would allocate 80% of the data for training and 20% for testing. While random splitting is generally preferred, to ensure consistency and comparability of results, we used images 1 to 8 as the training set and images 9 to 10 as the test set.

Validation methods

The ultimate goal of this research is to produce a binary image that can be compared to the original ground truth annotations using the F1 score. This metric, calculated as the harmonic mean of precision and recall, will assess the accuracy of the image segmentation by quantifying the number of misclassified pixels—both black pixels identified as white and white pixels identified as black.

$$F1 - score = 2 * \frac{Precision * Recall}{Precision + Recall}$$

Minimum thresholding

Minimum Thresholding is a technique used in image segmentation to separate objects from the background by identifying a threshold value based on the intensity histogram of the image. The threshold is chosen as the minimum value between two prominent peaks in the histogram, which typically represent the background and the object regions.

This approach assumes that the image has bimodal intensity distributions (one peak for the background and one for the object) and the intensity values at the minimum between these peaks correspond to the threshold that best separates them.

Segmentation implementation

Method 1: Reconstruction by dilation

This method aims to reconstruct the image from clearly defined markers by retaining only the pores of interest and removing background noise. The steps involved are as follows:

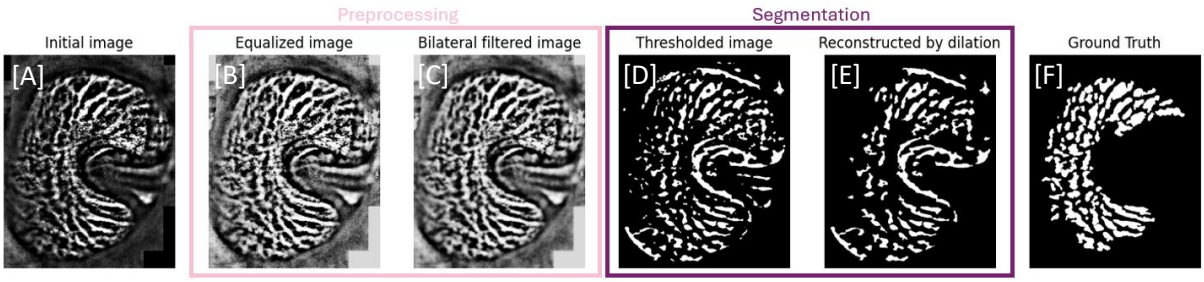

Figure 3: Illustration of the different processing and segmenting steps on image LC003 to obtain a binary result image with the reconstruction by dilation method

1. **Load the Images (figure 3A) and Ground Truth Masks (figure 3F)**: Begin by loading the images and their corresponding ground truth masks for processing. These masks serve as a benchmark for evaluating the performance of the detection method.
2. **Replace Black Rectangle Pixel Values**: Replace pixel values within black rectangles with a median gray value (in our case 128) to ensure these areas do not affect thresholding.
3. **Equalize Image Histograms (figure 3B)**: Perform histogram equalization to normalize contrast across images, enabling uniform application of thresholds or adjustments.
4. **Apply Bilateral Filter (figure 3C)**: Use a bilateral filter to smooth out the pores' edges, enhancing the outline and the distinguishability of the pores.
5. **Re-Equalize the Histograms**: Reapply histogram equalization to maximize the dynamic range. The resulting image is referred to as the *equalized bilateral image* and has pixel values normalized between 0 and 1. Then, two parallel processes are executed:
    a. **Manual Thresholding (figure 3D)**: Apply a manual threshold at 0.155 (determined by combing through 30 thresholds) to the equalized bilateral image. This threshold is chosen to detect pores while minimizing noise.

b. **Local Minima Detection (figure 4A)**: Identify local minima in the *equalized bilateral image*.

6. **Create Markers (figure 4B)**: Generate markers by multiplying the manually thresholded image with the local minima image. This step uses the manual threshold as a mask to suppress noise retained by the local minima on the image's far edges.
7. **Refine Markers via Erosion (figure 4C)**: Refine the markers by applying erosion using a square structuring element (SE) of size 3 to minimize side noise further.
8. **Reconstruct the Image by Dilation (figure 3E)**: Finally, reconstruct the image by dilation using the refined markers, and evaluate the F1-score by comparing the results against the ground truth.

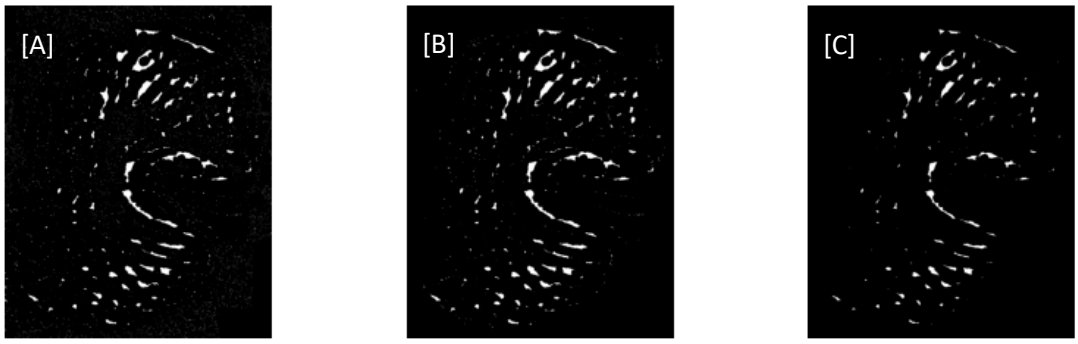

Figure 4: [A] Local minima [B] Manually thresholded image applied as a mask to the local minimum [C] Eroded thresholded image with a square structuring element of 2x2

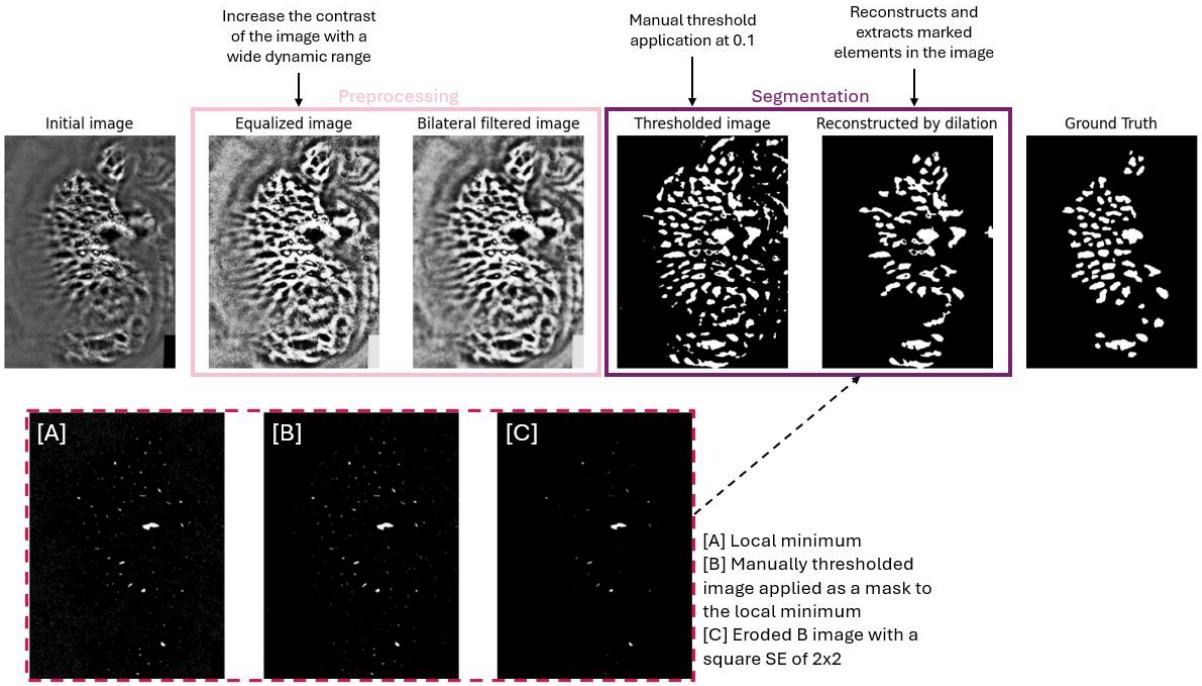

Figure 5: Illustration of the different processing and segmenting steps on image LC001 to obtain a binary result image with the reconstruction by dilation method

Method 2: Top Hat

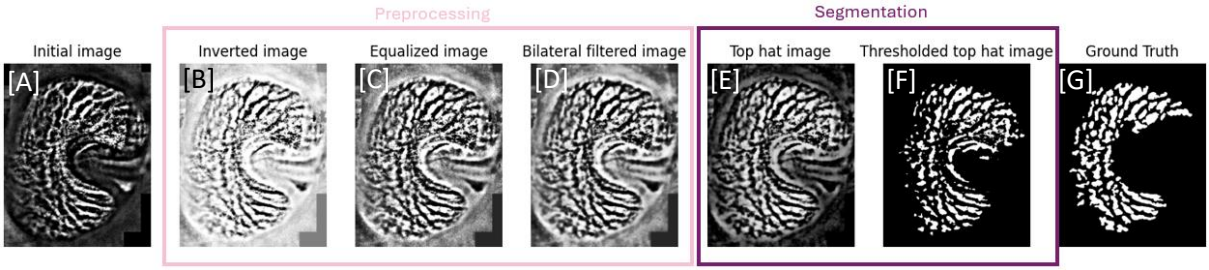

Figure 6: Illustration of the different processing and segmenting steps on image LC003 to obtain a binary result image with the top hat method

This method employs the morphological Top Hat operation to enhance and isolate the pores by removing background structures and improving the contrast between the pores and their surroundings. The steps involved are as follows:

1. **Load the Images (figure 6A) and Ground Truth Masks (figure 6G)**: Begin by loading the images and their corresponding ground truth masks for processing. These masks serve as a benchmark for evaluating the performance of the detection method.
2. **Replace Black Rectangle Pixel Values**: Replace pixel values within black rectangles with a median gray value (128) to ensure these regions do not interfere with the Top Hat operation.
3. **Invert Image Intensities (figure 6B)**: The gray levels in the image are inverted using a bitwise NOT operation. This inversion makes the dark features (pores) appear bright, which is suitable for the Top Hat operation.
4. **Equalize the Histogram (figure 6C)**: Perform histogram equalization to normalize the intensity distribution across the image. This step enhances the contrast between the inverted pores and the background
5. **Apply Bilateral Filter**: Use a bilateral filter to smooth out the pores' edges, enhancing the outline and the distinguishability of the pores.
6. **Re-Equalize the Histogram (figure 6D)**: Reapply histogram equalization to maximize the dynamic range. The resulting image is referred to as the *equalized bilateral image*.
7. **Morphological Top Hat Operation (figure 6E)**: A rectangular structuring element (SE) of size 65x65 is created (determined by combing through 30 size of SE). The Top Hat operation is applied using this SE and gives an image normalized between 0 and 1. The Top Hat operation highlights regions that are smaller and brighter than the structuring element, effectively isolating the pores.
8. **Manual Thresholding (figure 6F)**: The output of the Top Hat operation is processed using a manually determined threshold value of 0.717 (identified through analysis of 12 samples). Pixels below this threshold are set to 1 (indicating the presence of pores), and others are set to 0 (background). Then we evaluate the F1-score by comparing the results against the ground truth.

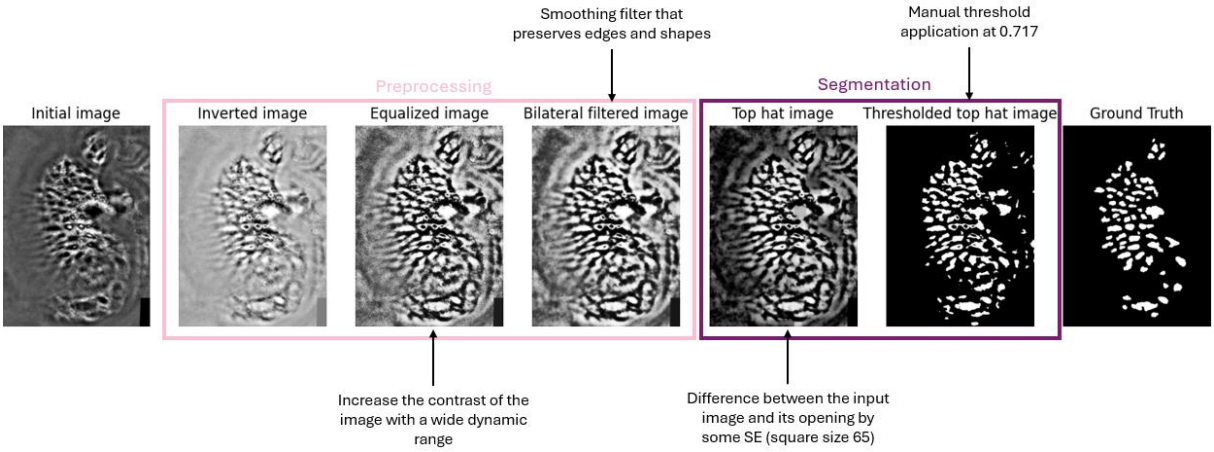

Figure 7: Illustration of the different processing and segmenting steps on image LC001 to obtain a binary result image with the top hat method

Method 3: Top Hat Variant

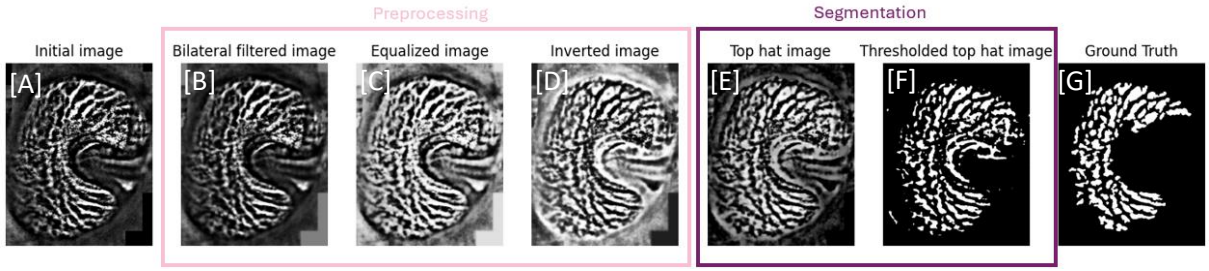

Figure 8: Illustration of the different processing and segmenting steps on image LC003 to obtain a binary result image with the second top hat method

This method employs the morphological Top Hat operation to enhance and isolate the pores by removing background structures and improving the contrast between the pores and their surroundings. The steps involved are as follows:

1. **Load the Images (figure 8A) and Ground Truth Masks (figure 8G)**: Start by loading the images and their corresponding ground truth masks. These masks are used as a reference to evaluate the detection performance.
2. **Replace Black Rectangle Pixel Values**: Modify pixel values within black rectangles to a median gray value (128) to prevent interference during the Top Hat operation.
3. **Apply Bilateral Filter (figure 8B)**: Use a bilateral filter to smooth the image, enhancing the edges of the pores while preserving significant details.
4. **Equalize the Histogram (figure 8C):** Perform histogram equalization on the filtered image to normalize the intensity distribution and enhance contrast.
5. **Invert Image Intensities (figure 8D)**: Invert the gray levels in the image using a bitwise NOT operation, making the dark features (pores) appear bright.

6. **Apply Morphological Top Hat Operation (figure 8E)**: Create a rectangular structuring element (SE) of size 59×59 and apply the Top Hat operation to extract the bright features (pores) from the background.
7. **Threshold the Output**: Apply a minimum thresholding operation to the Top Hat result using a predefined threshold rate. Convert the resulting binary image to an 8-bit format for compatibility, where pores are represented as white (1) and the background as black (0).

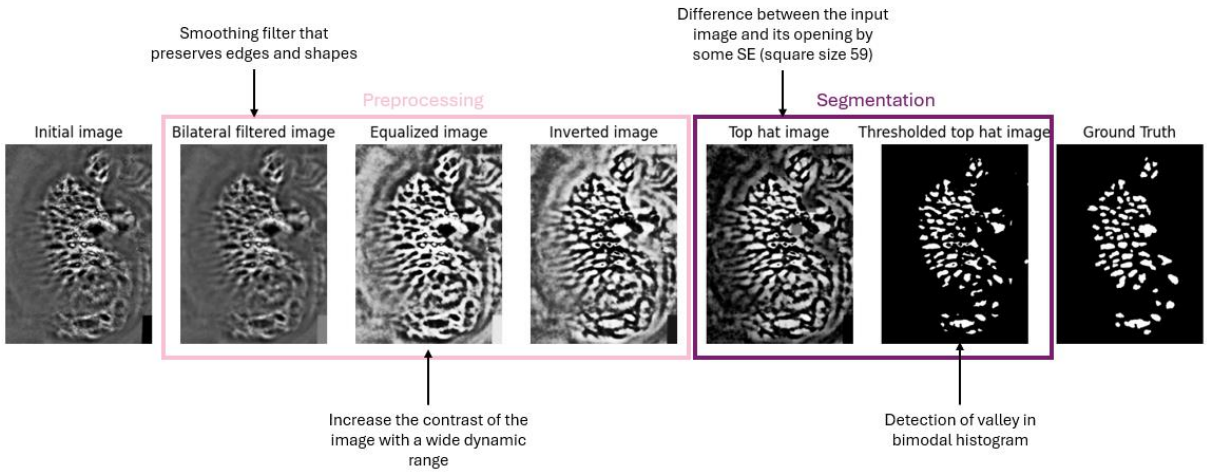

Figure 9: Illustration of the different processing and segmenting steps on image LC001 to obtain a binary result image with the second top hat method

Results and discussion

The following figures depict the comparison between the end result of each method applied to images 1 (LC001) and 3 (LC003), and their corresponding ground truth. The difference was computed between each pair of images and plotted using different colors (indicated in a color bar next to the plots): red for segments that should not be on the results, meaning that some regions out of the ROI were segmented; green for regions with no difference, corresponding to a perfect coincidence between segments or background exists in both the result and the ground truth; and blue for regions missing on the results, implying regions of the ROI that are incomplete.

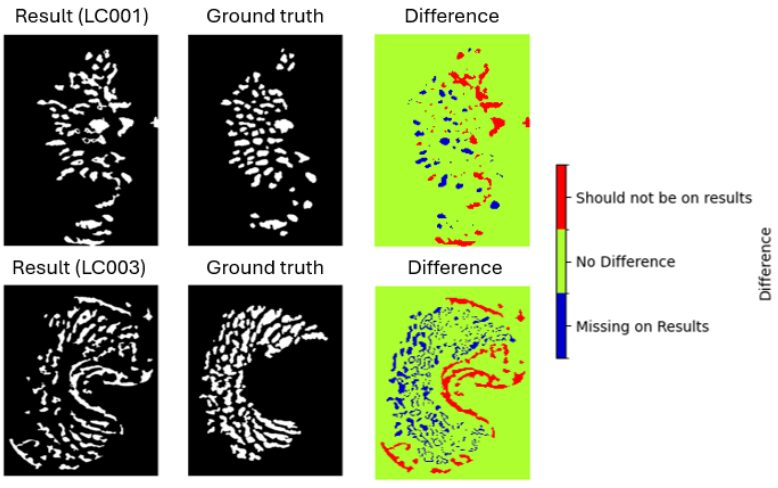

Figure 10: Method 1 (Reconstruction by dilation). Difference between end result and ground truth on images LC001 and LC003.

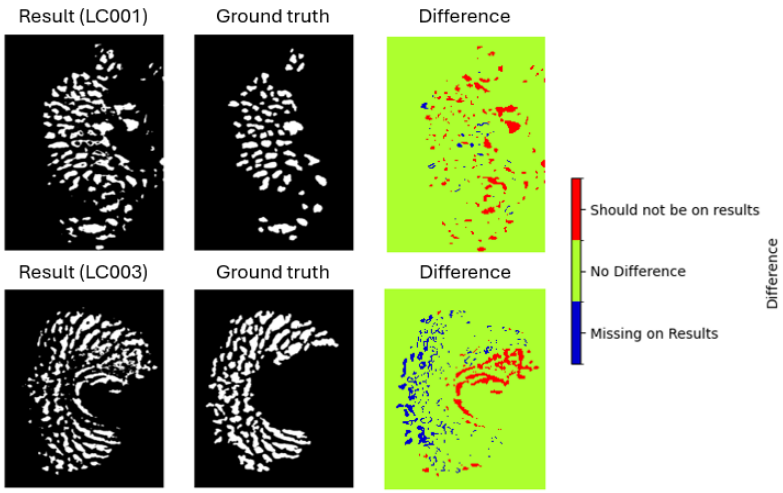

Figure 11: Method 2 (Top hat 1). Difference between end result and ground truth on images LC001 and LC003.

Figure 12: Method 3 (Top hat 2). Difference between end result and ground truth on images LC001 and LC002.

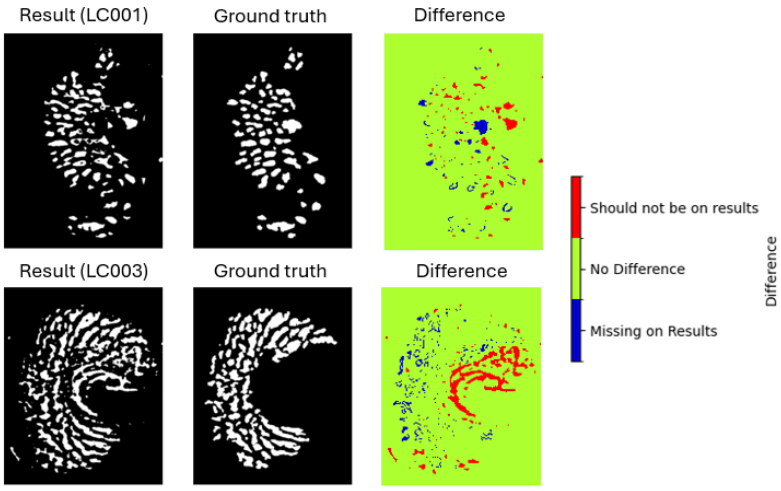

The difference images clearly show that image 3 consistently retains large elements that should not appear in the results. These elements are not pores and should be removed, potentially using alternative methods. So far, such elements have typically been removed manually in studies by applying hand-drawn masks, but the objective would be to automate this process.

The table below summarizes the F1-scores obtained for each of the three methods:

	Method 1		Method 2		Method 3	
F1-score	μ	σ	μ	σ	μ	σ
Training set	0.621	0.074	0.749	0.049	0.737	0.035
Test set	0.584	0.021	0.774	0.022	0.728	0.051

From these results, it is clear that the reconstruction-based method (Method 1) performs significantly worse than the two Top Hat-based methods. While the reconstruction method shows potential and could be developed further, it is not suitable as the preferred approach in its current form.

The Top Hat methods (Methods 2 and 3) yield similar performance and provide satisfactory results for this mini project. However, their accuracy may not be sufficient for more advanced applications, such as detecting glaucoma by analyzing the shapes of pores. Improvements or alternative approaches would likely be needed for such medical applications.

Conclusion

In conclusion, the project demonstrates that top hat methods effectively approximate ground truth, both when coupled with manual and minimum thresholding. This approach has shown significant potential in improving image segmentation accuracy.

For future perspectives, the focus will be on refining post-processing techniques, specifically improving large region elimination, which is currently done in existing articles using manual masks. Furthermore, integrating machine learning models such as U-net presents a promising direction for automating and enhancing segmentation tasks, enabling more robust and scalable solutions.

While the immediate goal of this project was image segmentation, its broader aim is to calculate the circularity of pores. According to recent studies, pore circularity could serve as a biomarker for glaucoma detection in patients. To achieve this, further steps could include coding the circularity calculation in Python or using existing tools like ImageJ for advanced analysis.

Bibliography

Zwillinger, S et al. “In vivo characterization of lamina cribrosa pore morphology in primary open-angle glaucoma.” *Journal français d'ophtalmologie* vol. 39,3 (2016): 265-71. doi:10.1016/j.jfo.2015.11.006

Park, Sung Chul & Ritch, Robert. (2011). High resolution in vivo imaging of the lamina cribrosa. Saudi journal of ophthalmology : official journal of the Saudi Ophthalmological Society. 25. 363-72. DOI : 10.1016/j.sjopt.2011.07.007. (https://www.researchgate.net/publication/255987668_High_resolution_in_vivo_imaging_of_the_lamina_cribrosa)

Nadler, Z. et al. “Automated lamina cribrosa microstructural segmentation in optical coherence tomography scans of healthy and glaucomatous eyes. ”. Biomedical Optics Express, Vol 4., No. 11 (2013). DOI:10.1364/BOE.4.002596